

# A comparison of different order hybrid finite difference-volume for the Serre equations in conservative form

Jordan Pitt,<sup>1</sup> Not a Member, ASCE  
Christopher Zoppou,<sup>1</sup> Member, ASCE  
Stephen G. Roberts,<sup>1</sup> Not a Member, ASCE

## ABSTRACT

**Keywords:** dispersive waves, conservation laws, Serre equation, shallow water wave equations, finite volume method, finite difference method

## <sup>1</sup> INTRODUCTION

<sup>2</sup> [credit derivars]

## <sup>3</sup> SERRE EQUATIONS

<sup>4</sup> The Serre equations can derived as an approximation to the full Euler equations by  
<sup>5</sup> depth integration similar to (Su and Gardner 1969). They can also be seen as an asymptotic  
<sup>6</sup> expansion to the Euler equations as well (Lannes and Bonneton 2009). The former is more  
<sup>7</sup> consistent with the perspective from which numerical methods will be developed while the  
<sup>8</sup> latter indicates the appropriate regions in which to use these equations as a model for fluid  
<sup>9</sup> flow. The set up of the scenario under which the Serre approximation is made consists of  
<sup>10</sup> a two dimensional  $\mathbf{x} = (x, z)$  fluid over a bottom topography as in Figure 1 acting under  
<sup>11</sup> gravity. Consider a fluid particle at depth  $\xi(\mathbf{x}, t) = z - h(x, t) - z_b(x)$  below the water  
<sup>12</sup> surface, see Figure 1. Where the water depth is  $h(x, t)$  and  $z_b(x)$  is the bed elevation. The  
<sup>13</sup> fluid particle is subject to the pressure,  $p(\mathbf{x}, t)$  and gravitational acceleration,  $\mathbf{g} = (0, g)^T$   
<sup>14</sup> and has a velocity  $\mathbf{u} = (u(\mathbf{x}, t), w(\mathbf{x}, t))$ , where  $u(\mathbf{x}, t)$  is the velocity in the  $x$ -coordinate and  
<sup>15</sup>  $w(\mathbf{x}, t)$  is the velocity in the  $z$ -coordinate and  $t$  is time. Assuming that  $z_b(x)$  is constant the  
<sup>16</sup> Serre equations read (Li et al. 2014)

$$\frac{\partial h}{\partial t} + \frac{\partial(\bar{u}h)}{\partial x} = 0 \quad (1a)$$

$$\underbrace{\frac{\partial(\bar{u}h)}{\partial t} + \frac{\partial}{\partial x} \left( \bar{u}^2 h + \frac{gh^2}{2} \right)}_{\text{Shallow Water Wave Equations}} + \underbrace{\frac{\partial}{\partial x} \left( \frac{h^3}{3} \left[ \frac{\partial \bar{u}}{\partial x} \frac{\partial \bar{u}}{\partial x} - \bar{u} \frac{\partial^2 \bar{u}}{\partial x^2} - \frac{\partial^2 \bar{u}}{\partial x \partial t} \right] \right)}_{\text{Dispersion Terms}} = 0. \quad (1b)$$

Serre Equations

<sup>1</sup>Mathematical Sciences Institute, Australian National University, Canberra, ACT 0200, Australia, E-mail: Jordan.Pitt@anu.edu.au. The work undertaken by the first author was supported financially by an Australian National University Postgraduate Research Award.

22 Where  $\bar{u}$  means the average of  $u$  over the depth of water.

23 **Alternative Conservation Law Form of the Sere Equations**

24 In (Le Métayer et al. 2010; Li et al. 2014) it is demonstrated that the Serre equations  
25 can be rearranged into a conservation law form, by the addition of a new quantity  $G$ .

26

$$G = uh - h^2 \frac{\partial h}{\partial x} \frac{\partial u}{\partial x} - \frac{h^3}{3} \frac{\partial^2 u}{\partial x^2}. \quad (2)$$

27

28 Consequently the equations can be rewritten as

29

$$\frac{\partial h}{\partial t} + \frac{\partial(uh)}{\partial x} = 0, \quad (3a)$$

30

31

$$\frac{\partial G}{\partial t} + \frac{\partial}{\partial x} \left( Gu + \frac{gh^2}{2} - \frac{2h^3}{3} \frac{\partial u}{\partial x} \frac{\partial u}{\partial x} \right) = 0. \quad (3b)$$

32

33 Where the bar over  $u$  has been dropped for ease of notation. This opens the Serre equations  
34 up to a hybrid method that for each time step solves the elliptic problem (2) for  $u$  and then  
35 the conservation law (3) with a finite volume method. As was done in (Le Métayer et al.  
36 2010).

37

38 **NUMERICALLY SOLVING THE SERRE EQUATIONS WRITTEN IN  
39 CONSERVATION LAW FORM**

40 There are numerous ways a numerical method could be built to solve the Serre equa-  
41 tions, in this form and allowing for discontinuities a finite volume method seems the most  
42 appropriate. Such a method can now be applied due to the rearranging of the equations  
43 performed above. However, it can only handle the equation (3), to show how (2) can also  
44 be used some notation will be introduced. Consider a discretisation in time that will be  
45 denoted by superscript, for instance  $h^n \approx h(x, t^n)$ . Now consider a finite volume method to  
46 solve (3) that is any order in space and time; it updates the conserved quantities  $h$  and  $G$   
47 from time  $t^n$  to  $t^{n+1}$ . Such a method would act like so

48

$$\begin{bmatrix} h^{n+1} \\ G^{n+1} \end{bmatrix} = \mathcal{L}(h^n, G^n, u^n, \Delta t). \quad (4)$$

49

50 Where  $\mathcal{L}$  is the numerical solver for (3) that does a single time step  $\Delta t$ . Clearly it can be  
51 seen that in addition to  $\mathcal{L}$  another method is required that solves for  $u^n$  from  $h^n$  and  $G^n$ .  
52 Indeed using a numerical method to solve for  $u$  in (2) using  $h$  and  $G$  would give such a  
53 method, it would act like so

54

$$u = \mathcal{A}(h, G). \quad (5)$$

55

56 Thus given  $h^n$  and  $G^n$  a time step that gives these conserved quantities at  $t^{n+1}$  is given by:

57  $u^n = \mathcal{A}(h^n, G^n),$

59

60 
$$\begin{bmatrix} h^{n+1} \\ G^{n+1} \end{bmatrix} = \mathcal{L}(h^n, G^n, u^n, \Delta t).$$

62 Where  $\mathcal{L}$  can be a finite volume method because of the rearrangement of the equations and  
63 can thus handle discontinuities in the conserved variables.

64 **METHOD FOR  $\mathcal{A}$**

65 In the above section a very general map of a typical time step in these hybrid methods  
66 for the Serre equations and a discretisation in time were given. In this paper a fully discrete  
67 system will be built hence a discretisation of space is also introduced, denoted by subscript  
68  $i$  for example  $h_i^n \approx h(x_i, t^n)$ . Additionally assume that this discretisation in space is fixed  
69 so that  $\forall i x_{i+1} - x_i = \Delta x$ . For a fixed time (2) is just an ordinary differential equation,  
70 thus it seems reasonable that solving a finite difference approximation of it would give a  
71 satisfactory method for  $\mathcal{A}$ . Since the goal of this paper is to develop and compare a  
72 range of different order methods for this problem both a second- and fourth-order centred  
73 finite difference approximation will be given for (2). These are approximations are as  
74 follows

75 
$$\left( \frac{\partial h}{\partial x} \right)_i = \frac{h_{i+1} - h_{i-1}}{2\Delta x}, \quad (6)$$

76

77 
$$\left( \frac{\partial h}{\partial x} \right)_i = \frac{-h_{i+2} + 8h_{i+1} - 8h_{i-1} + h_{i-2}}{12\Delta x}, \quad (7)$$

80 which are second- and fourth-order in space respectively. Likewise a second- and fourth-  
81 order central finite difference is applied to the double space derivative respectively

82 
$$G_i = u_i h_i - h_i^2 \left( \frac{h_{i+1} - h_{i-1}}{2\Delta x} \right) \left( \frac{u_{i+1} - u_{i-1}}{2\Delta x} \right) - \frac{h_i^3}{3} \left( \frac{u_{i+1} - 2u_i + u_{i-1}}{\Delta x^2} \right), \quad (8)$$

83

84 
$$G_i = u_i h_i - h_i^2 \left( \frac{-h_{i+2} + 8h_{i+1} - 8h_{i-1} + h_{i-2}}{12\Delta x} \right) \left( \frac{-u_{i+2} + 8u_{i+1} - 8u_{i-1} + u_{i-2}}{12\Delta x} \right) \quad (9)$$
  
85 
$$- \frac{h_i^3}{3} \left( \frac{-u_{i+2} + 16u_{i+1} - 30u_i + 16u_{i-1} - u_{i-2}}{12\Delta x^2} \right).$$

86

87 Both of these can be rearranged into a matrix equation with the following form

$$88 \quad \begin{bmatrix} G_0 \\ \vdots \\ G_m \end{bmatrix} = A \begin{bmatrix} u_0 \\ \vdots \\ u_m \end{bmatrix}.$$

90 Where  $A$  will also use values at time  $t^n$ . For a second-order approximation the matrix  $A$   
 91 is tri-diagonal while for a fourth-order scheme  $A$  is penta-diagonal. Thus two methods of  
 92 satisfactory order in space has been devised to solve the elliptic problem (2) in the Serre  
 93 equations.

#### 94 **METHOD FOR $\mathcal{L}$**

95 A finite volume method of sufficient order was developed to solve (3). Importantly  
 96 finite volumes have a different discretion of space, so a new notation is introduced which  
 97 will now be demonstrated by example

$$98 \quad \bar{h}_i = \frac{1}{\Delta x} \int_{x_{i-\frac{1}{2}}}^{x_{i+\frac{1}{2}}} h(x, t) dx.$$

100 Where  $x_{i\pm\frac{1}{2}} = x_i \pm \frac{\Delta x}{2}$ . Finite volume schemes work with these cell averaged values and  
 101 give them as outputs by the following scheme

$$102 \quad \bar{\mathbf{U}}_i^{n+1} = \bar{\mathbf{U}}_i^n - \frac{\Delta t}{\Delta x} \left( \mathbf{F}_{i+\frac{1}{2}}^n - \mathbf{F}_{i-\frac{1}{2}}^n \right).$$

104 Where  $\bar{\mathbf{U}}_i^n$  is an approximation of the vector of the conserved quantities averaged over the  
 105 cell at time  $t^n$  in this case  $\bar{\mathbf{U}}_i^n = \begin{bmatrix} \mathbf{h}_i^n \\ \mathbf{G}_i^n \end{bmatrix}$ . While  $\mathbf{F}_{i\pm\frac{1}{2}}^n$  is an approximation of the average  
 106 flux at  $x_{i\pm\frac{1}{2}}$  over the time interval  $[t^n, t^{n+1}]$  which is given by approximating the Riemann  
 107 problem at the cell boundaries. The values to the left and right of a cell edge say  $x_{i+\frac{1}{2}}$  are  
 108 reconstructed by assuming appropriate order polynomials over each cell. For example for  
 109  $h$  this would result in  $h_{i+\frac{1}{2}}^-$  and  $h_{i+\frac{1}{2}}^+$  for the left and right reconstructed values at  $x_{i+\frac{1}{2}}$ .

#### 110 *Reconstruction*

111 The order of the polynomials used to reconstruct the quantities inside the cell deter-  
 112 mines the order of the scheme in space. In Godunov's original formulation of the method  
 113 (Godunov 1959) the polynomials are constant functions resulting in a first-order method.  
 114 Similarly first- and second-degree polynomials result in second- and third-order schemes.

115 To make this section easier the following notation is introduced  $P_i^k$  denotes the polynomial  
 116 of degree  $k$  for any quantity  $q$  over the interval with  $x_i$  as its midpoint. Thus for a  
 117 zero-degree polynomial the reconstruction formula is

$$118 \quad P_i^0 = \bar{q}_i = q_i. \quad (10)$$

120 However for higher degree polynomials the extra degrees of freedom mean that choices  
 121 have to be made to decide the behaviour of the fitted polynomial. For linear functions the  
 122 midpoint of a quantity on an interval and the average of the quantity over the interval are  
 123 the same. Thus the natural choice for the slope of  $P_i^1$  is the slope between the midpoints  
 124 of the two neighbouring cells. While for third-order it is reasonable to use the degrees  
 125 of freedom so that the polynomial has the correct average value over its corresponding  
 126 cell and its two neighbours either side. However to suppress non-physical oscillations  
 127 limiting must be implemented. For the second-order scheme the minmod limiter was used  
 128 as in (Kurganov et al. 2002), while for the third-order scheme the Koren limiter was used  
 129 (Koren 1993). This results in the following fitting schemes respectively

$$130 \quad P_i(x) = a_i(x - x_i) + q_i, \quad (11a)$$

132

$$133 \quad a_i = \text{minmod} \left\{ \theta \frac{q_{i+1} - q_i}{\Delta x}, \frac{q_{i+1} - q_{i-1}}{2\Delta x}, \theta \frac{q_i - q_{i-1}}{\Delta x} \right\} \quad \text{for } \theta \in [1, 2] \quad (11b)$$

135

$$136 \quad r_i = \frac{\bar{q}_{i+1} - \bar{q}_i}{\bar{q}_i - \bar{q}_{i-1}} \quad (12a)$$

137

$$138 \quad q_{i+\frac{1}{2}}^- = \bar{q}_i + \frac{1}{2} \phi^-(r_i) (\bar{q}_i - \bar{q}_{i-1}) \quad (12b)$$

139

140

141

$$142 \quad q_{i+\frac{1}{2}}^+ = \bar{q}_i - \frac{1}{2} \phi^+(r_i) (\bar{q}_i - \bar{q}_{i-1}) \quad (12c)$$

143

144

$$145 \quad \phi^-(r_i) = \max \left[ 0, \min \left[ 2r_i, \frac{1+2r_i}{3}, 2 \right] \right] \quad (12d)$$

146

147

$$148 \quad \phi^+(r_i) = \max \left[ 0, \min \left[ 2r_i, \frac{2+r_i}{3}, 2 \right] \right] \quad (12e)$$

150 *Local Riemann Problem*

151 Since  $\bar{U}_i^n$  is known what remains in the equations is to calculate the two fluxes. As  
 152 stated above this is done by approximating the Riemann problem, in (Kurganov et al.  
 153 2002) the following formula is derived

$$154 \quad F_{i+\frac{1}{2}} = \frac{a_{i+\frac{1}{2}}^+ f\left(q_{i+\frac{1}{2}}^-\right) - a_{i+\frac{1}{2}}^- f\left(q_{i+\frac{1}{2}}^+\right)}{a_{i+\frac{1}{2}}^+ - a_{i+\frac{1}{2}}^-} + \frac{a_{i+\frac{1}{2}}^+ a_{i+\frac{1}{2}}^-}{a_{i+\frac{1}{2}}^+ - a_{i+\frac{1}{2}}^-} \left[ q_{i+\frac{1}{2}}^+ - q_{i+\frac{1}{2}}^- \right]. \quad (13)$$

155 Where  $f$  is just the flux function of the conservative law for quantity  $q$ . While  $a_{i+\frac{1}{2}}^+$  and  
 $a_{i+\frac{1}{2}}^-$  are given by

$$156 \quad a_{i+\frac{1}{2}}^+ = \max \left[ \lambda_2 \left( q_{i+\frac{1}{2}}^- \right), \lambda_2 \left( q_{i+\frac{1}{2}}^+ \right), 0 \right], \quad (14a)$$

$$157 \quad a_{i+\frac{1}{2}}^- = \min \left[ \lambda_1 \left( q_{i+\frac{1}{2}}^- \right), \lambda_1 \left( q_{i+\frac{1}{2}}^+ \right), 0 \right]. \quad (14b)$$

158 Where  $\lambda_1$  and  $\lambda_2$  are estimates of the smallest and largest eigenvalues respectively of the  
 159 Jacobian which corresponds to the phase speeds.

160 *Propagation Speeds of a Local Shock*

161 As noted in (Le Métayer et al. 2010) [] the phase speeds are bounded from above and  
 162 below by the phase speed of the Shallow Water Wave Equations, so that

$$162 \quad \lambda_1 := u - \sqrt{gh} \leq v_p \leq u + \sqrt{gh} =: \lambda_2. \quad (15)$$

163 Thus  $a_{i+\frac{1}{2}}^+$  and  $a_{i+\frac{1}{2}}^-$  are fully determined.

164 *Fully discrete approximations to flux function*

165 For height the fully discrete any order approximation to  $f(h_{i+\frac{1}{2}}^-)$  and  $f(h_{i+\frac{1}{2}}^+)$  are clear  
 166 and given by

$$167 \quad f \left( h_{i+\frac{1}{2}}^- \right) = u_{i+\frac{1}{2}}^- h_{i+\frac{1}{2}}^-, \quad (16a)$$

$$170 \quad f \left( h_{i+\frac{1}{2}}^+ \right) = u_{i+\frac{1}{2}}^+ h_{i+\frac{1}{2}}^+. \quad (16b)$$

172 For  $G$  this is complicated by a derivative, leaving a general place holder for an approxima-  
 173 tion to the derivative it looks like so

174

$$f\left(G_{i+\frac{1}{2}}^{-}\right) = u_{i+\frac{1}{2}}^{-} G_{i+\frac{1}{2}}^{-} + \frac{g\left(h_{i+\frac{1}{2}}^{-}\right)^2}{2} - \frac{2\left(h_{i+\frac{1}{2}}^{-}\right)^3}{3} \left[\left(\frac{\partial u}{\partial x}\right)_{i+\frac{1}{2}}^{-}\right]^2, \quad (17a)$$

175

176

177

$$f\left(G_{i+\frac{1}{2}}^{+}\right) = u_{i+\frac{1}{2}}^{+} G_{i+\frac{1}{2}}^{+} + \frac{g\left(h_{i+\frac{1}{2}}^{+}\right)^2}{2} - \frac{2\left(h_{i+\frac{1}{2}}^{+}\right)^3}{3} \left[\left(\frac{\partial u}{\partial x}\right)_{i+\frac{1}{2}}^{+}\right]^2. \quad (17b)$$

178

179 There are multiple ways to approximate this derivative with different corresponding orders  
 180 of accuracy. The first- and third-order approximations are the most natural and come from  
 181 upwind finite difference approximations [] while the second-order choice is an intuitive  
 182 choice that has the correct order and is simpler to implement than its corresponding up-  
 183 wind finite difference approximation. Thus there are the following approximations to the  
 184 derivatives

185

$$\left(\frac{\partial u}{\partial x}\right)_{i+\frac{1}{2}}^{+} = \frac{u_{i+\frac{3}{2}}^{+} - u_{i+\frac{1}{2}}^{+}}{\Delta x}, \quad (18a)$$

186

187

188

$$\left(\frac{\partial u}{\partial x}\right)_{i+\frac{1}{2}}^{-} = \frac{u_{i+\frac{1}{2}}^{-} - u_{i-\frac{1}{2}}^{-}}{\Delta x}, \quad (18b)$$

189

190

191

$$\left(\frac{\partial u}{\partial x}\right)_{i+\frac{1}{2}}^{-} = \left(\frac{\partial u}{\partial x}\right)_{i+\frac{1}{2}}^{+} = \frac{u_{i+1} - u_i}{\Delta x}, \quad (19)$$

192

193

194

$$\left(\frac{\partial u}{\partial x}\right)_{i+\frac{1}{2}}^{+} = \frac{-u_{i+\frac{3}{2}}^{+} + 4u_{i+\frac{1}{2}}^{+} - 3u_{i-\frac{1}{2}}^{+}}{\Delta x}, \quad (20a)$$

195

196

197

$$\left(\frac{\partial u}{\partial x}\right)_{i+\frac{1}{2}}^{-} = \frac{3u_{i+\frac{1}{2}}^{-} - 4u_{i-\frac{1}{2}}^{-} + u_{i-\frac{3}{2}}^{-}}{\Delta x}, \quad (20b)$$

198

199 For the first-, second- and third-order schemes respectively.

## 200 Transforming between midpoints and averages

Notice that the schemes for  $\mathcal{L}$  uses cell averages and values at the cell boundaries based on the reconstruction. While  $\mathcal{A}$  uses fixed points at the cell centres, thus between applying the two schemes a transformation from the cell averages to the cell centres must be made. For the first- and second-order schemes this distinction is trivial since  $\bar{q}_i = q_i$  so both operations work with the same values. However for third-order schemes this is a very important distinction and failure to handle this will result in a loss of accuracy. For this problem it is enough to go back to the intuitive quadratic polynomial to fit on the interval centred at  $x_i$  so that the polynomial also gives the correct cell averages for the two neighbouring cells. This results in the following

$$q_i = \frac{-\bar{q}_{i+1} + 26\bar{q}_i - \bar{q}_{i-1}}{24}. \quad (21)$$

212 Thus one can form a tri-diagonal matrix equation between the vector of all midpoint values  
 213 and all cell average values and use the resultant transformation matrix to go back and forth.  
 214 For convenience denote the transformation from midpoints to cell averages by  $\mathcal{M}$  while  
 215 the inverse matrix operation transforming from cell averages to midpoints will be denoted  
 216 by  $\mathcal{M}^{-1}$ . This completes the effort to build a single time step for the system denotes by  $\mathcal{H}$   
 217 of equations which is now as follows

$$\begin{bmatrix} \mathbf{h}^n \\ \mathbf{G}^n \end{bmatrix} = \begin{bmatrix} \mathcal{M}^{-1}(\bar{\mathbf{h}}^n) \\ \mathcal{M}^{-1}(\bar{\mathbf{G}}^n) \end{bmatrix}$$

$$u^n \equiv \mathcal{A}(h^n, G^n),$$

$$\begin{bmatrix} \bar{h}^n \\ \bar{G}^n \\ \bar{u}^n \end{bmatrix} = \begin{bmatrix} \mathcal{M}(h^n) \\ \mathcal{M}(G^n) \\ \mathcal{M}(u^n) \end{bmatrix}$$

$$\begin{bmatrix} \bar{\boldsymbol{h}}^{n+1} \\ \bar{\boldsymbol{G}}^{n+1} \end{bmatrix} = \mathcal{L}(\bar{\boldsymbol{h}}^n, \bar{\boldsymbol{G}}^n, \bar{\boldsymbol{u}}^n, \Delta t).$$

229 Strong-Stability-Preserving Runge-Kutta Scheme

<sup>230</sup> The time step above is first-order accurate there are many methods to increase the  
<sup>231</sup> accuracy of such a method in time, this paper will follow the SSP RK steps as in (Gottlieb  
<sup>232</sup> et al. 2009) to allow for fully second- and third-order schemes. These are constructed by

233 doing more of the time steps  $\mathcal{H}$  and then preforming a linear combinations of them. This  
 234 leads to the following schemes for first-, second- and third-order time stepping schemes  
 235 respectively

$$236 \quad \begin{bmatrix} \bar{\mathbf{h}}^{n+1} \\ \bar{\mathbf{G}}^{n+1} \end{bmatrix} = \mathcal{H}(\bar{\mathbf{h}}^n, \bar{\mathbf{G}}^n, \Delta t), \quad (22)$$

237

238

$$239 \quad \begin{bmatrix} \bar{\mathbf{h}}' \\ \bar{\mathbf{G}}' \end{bmatrix} = \mathcal{H}(\bar{\mathbf{h}}^n, \bar{\mathbf{G}}^n, \Delta t) \quad (23a)$$

240

241

$$242 \quad \begin{bmatrix} \bar{\mathbf{h}}'' \\ \bar{\mathbf{G}}'' \end{bmatrix} = \mathcal{H}(\bar{\mathbf{h}}', \bar{\mathbf{G}}', \Delta t) \quad (23b)$$

243

244

$$245 \quad \begin{bmatrix} \bar{\mathbf{h}}^{n+1} \\ \bar{\mathbf{G}}^{n+1} \end{bmatrix} = \frac{1}{2} \left( \begin{bmatrix} \bar{\mathbf{h}}^n \\ \bar{\mathbf{G}}^n \end{bmatrix} + \begin{bmatrix} \bar{\mathbf{h}}'' \\ \bar{\mathbf{G}}'' \end{bmatrix} \right), \quad (23c)$$

246

247

$$248 \quad \begin{bmatrix} \bar{\mathbf{h}}^{(1)} \\ \bar{\mathbf{G}}^{(1)} \end{bmatrix} = \mathcal{H}(\bar{\mathbf{h}}^n, \bar{\mathbf{G}}^n, \Delta t) \quad (24a)$$

249

250

$$251 \quad \begin{bmatrix} \bar{\mathbf{h}}^{(2)} \\ \bar{\mathbf{G}}^{(2)} \end{bmatrix} = \mathcal{H}(\bar{\mathbf{h}}^{(1)}, \bar{\mathbf{G}}^{(1)}, \Delta t) \quad (24b)$$

252

253

$$254 \quad \begin{bmatrix} \bar{\mathbf{h}}^{(3)} \\ \bar{\mathbf{G}}^{(3)} \end{bmatrix} = \frac{3}{4} \begin{bmatrix} \bar{\mathbf{h}}^n \\ \bar{\mathbf{G}}^n \end{bmatrix} + \frac{1}{4} \begin{bmatrix} \bar{\mathbf{h}}^{(2)} \\ \bar{\mathbf{G}}^{(2)} \end{bmatrix}, \quad (24c)$$

255

256

$$257 \quad \begin{bmatrix} \bar{\mathbf{h}}^{(4)} \\ \bar{\mathbf{G}}^{(4)} \end{bmatrix} = \mathcal{H}(\bar{\mathbf{h}}^{(3)}, \bar{\mathbf{G}}^{(3)}, \Delta t) \quad (24d)$$

258

259

$$260 \quad \begin{bmatrix} \bar{\mathbf{h}}^{(n+1)} \\ \bar{\mathbf{G}}^{(n+1)} \end{bmatrix} = \frac{1}{3} \begin{bmatrix} \bar{\mathbf{h}}^n \\ \bar{\mathbf{G}}^n \end{bmatrix} + \frac{2}{3} \begin{bmatrix} \bar{\mathbf{h}}^{(4)} \\ \bar{\mathbf{G}}^{(4)} \end{bmatrix}, \quad (24e)$$

261

262

263 **NUMERICAL SIMULATIONS**

264 The discussed methods will now be used to solve three different situations; analytic  
265 solution of the Serre equations given by the soliton, one of the experiments conducted by  
266 Segur and Hammack in (Hammack and Segur 1978) and a dam break problem from (El  
267 et al. 2006; Le Métayer et al. 2010). The first two will be for validation reasons with the  
268 first being to validate whether the scheme reproduces the soliton solution and the order  
269 of convergence while the second validates the behaviour of a shock against experimental  
270 data. Lastly the dam break will further investigate how the scheme handles shocks.

271 **Soliton**

272 Currently there is only one family of analytic solutions to the Serre equations which  
273 are cnoidal waves (Carter and Cienfuegos 2011). This solution has been used to verify the  
274 order of convergence of the proposed methods in this paper, in particular for the soliton  
275 case of this family. Solitons travel without deformation and in the Serre equations they  
276 have the following form

277 
$$h(x, t) = a_0 + a_1 \operatorname{sech}^2(\kappa(x - ct)), \quad (25a)$$

279

280 
$$u(x, t) = c \left( 1 - \frac{a_0}{h(x, t)} \right), \quad (25b)$$

281

282 
$$\kappa = \frac{\sqrt{3a_1}}{2a_0 \sqrt{a_0 + a_1}}, \quad (25c)$$

283

284 
$$c = \sqrt{g(a_0 + a_1)}. \quad (25d)$$

285

286 Where  $a_0$  and  $a_1$  are input parameters that determine the depth of the quiescent water and  
287 the maximum height of the soliton above that respectively. For the conducted simulation  
288  $a_0 = 10m$ ,  $a_1 = 1m$  over an  $x$  domain  $[-500m, 1500m]$  from time  $[0s, 100s]$ . Where  
289  $\Delta t = \lambda \Delta x$  and  $\lambda = 0.01$ . For second-order  $\theta = 1.2$ . The example results for  $\Delta x = 1.5625m$   
290 can be seen in Figures 3-5, while the relative error as measured by the L1-norm of the  
291 method can be seen in Figure 2.

292 Firstly Figure 2 demonstrates that the schemes all have the correct order of convergence  
293 in both time and space as desired since  $\Delta t = \lambda \Delta x$ . Clearly this order of convergence is  
294 not over all  $\Delta x$  the reason for this is when  $\Delta x$  is large the actual problem is not discretised  
295 well since the cells are too large to represent the simulation properly. Hence the order of  
296 convergence there will be significantly lower, this can be seen for all sub-figures of Figure

299 2. For Figure 2(c) there is also a decrease in the order of convergence, this is because the  
300 third-order scheme has become accurate enough for the floating point errors to become  
301 significant, thus the behaviour of the order of convergence for all methods is as good as  
302 one can expect.

303 Figures 3-5 demonstrate the superiority of the second- and third-order to the first-  
304 order method. This can also be seen in 2 where to get similar magnitude of the error for  
305 the first-order scheme and the higher order scheme requires a very small  $\Delta x$  for the first  
306 order scheme. By inspecting the trailing edge of the soliton it can be seen that indeed as  
307 expected and supported by Figure 2 the third-order is better than the second-order method.  
308 With graphical inspection showing the third-order solution and the analytic solution to be  
309 identical on a relatively coarse grid with less than 500 cells representing the actual soliton.

310 Because of the added complexity of the higher order methods they do require more  
311 computational effort and hence are slower.[] Although the superior error does overcome  
312 this inefficiency.[]

### 313 Segur Laboratory Experiment

314 In (Hammack and Segur 1978) Hammack and Segur conducted an experiment that  
315 produced rectangular waves with the stroke of a  $0.61m$  long piston flush with the wall of  
316 a wave tank  $31.6m$  long and recorded the wave heights at certain positions over time. The  
317 quiescent water height  $h_1$  was  $0.1m$  while the stroke of the piston caused a depression of  
318 water  $h_0 = 0.095m$  deep. To run this as a numerical simulation the reflected problem must  
319 be used, the result of this is that the simulation is reflected around the origin and  $h_1 - h_0$  is  
320 doubled by changing  $h_0$ . Thus the domain is from  $-60m$  to  $60m$  and the simulation is run  
321 for  $50s$  with  $\Delta x = 0.01$ ,  $\lambda = \frac{0.2}{\sqrt{gh_1}}$  and  $\theta = 1.2$ . The results of this simulation are displayed  
322 in figures 6 - 8.

323 In this experiment the initial depression causes a right going rarefaction fan and a left  
324 going shock at least on the positive side of the axis. The two shocks then reflect in the  
325 middle and so the shock and the rarefaction fan are travelling in the same direction. The  
326 leading wave in all the related figures is that rarefaction fan while the trailing dispersive  
327 waves are the result of the reflected shock. The most important result of such a test is to  
328 investigate if the period of the produced waves are coherent with the experiment. Because  
329 things such as the wave heights, the number of waves and the speed of the waves will be  
330 different because real water has effects that the model ignores.

331 From all the related figures it can be seen that all models show good agreement be-  
332 tween the arrival of the first wave and the period of all the waves. While Figure 6 shows  
333 the first-order model is too diffusive and thus under approximates the wave heights of the  
334 dispersive waves of the shock. While the second- and third-order methods over approx-  
335 imate them. This discrepancy can be explained by the Serre equations not taking into

336 account viscous effects that diffuse the dispersive waves and so the Serre equations are  
 337 actually producing an upper bound on the wave heights for fluids with viscosity. These  
 338 experiments do validate the numerical schemes to correctly handle discontinuities. Also it  
 339 demonstrates that the oscillations produced by the schemes are physical.

340 **Dam Break**

341 The dam break problem can be defined as such

$$342 \quad h(x, 0) = \begin{cases} h_0 & x < x_m \\ h_1 & x \geq x_m \end{cases}, \quad (26)$$

343

344

$$345 \quad u(x, 0) = 0.0m/s. \quad (27)$$

347 For this problem the  $x$  domain was  $[0m, 1000m]$  while the simulation was run until  $t = 30s$ .  
 348 The other values were  $h_0 = 1.8m$ ,  $h_1 = 1.0m$ ,  $x_m = 500m$ ,  $\lambda = 0.01$  and  $\theta = 1.2$ .  
 349 This corresponds to sub-critical flow and was a situation demonstrated in (El et al. 2006;  
 350 Le Métayer et al. 2010). An example was plotted for  $\Delta x = 0.09765625m$  for all the  
 351 methods described in Figure 10. To determine if the oscillations that occur in the solution  
 352 indeed converge to some limit as  $\Delta x \rightarrow 0$  multiple  $\Delta x$  values must be used and then the  
 353 amount of variation in the solution measured. A common way to measure this is the total  
 354 variation  $TV$  (LeVeque 2002) which for a vector  $v$  of length  $k$  is given by

$$355 \quad TV(v) = \sum_{\forall i>1} |v_i - v_{i-1}|. \quad (28)$$

356

357 Importantly if the solution does indeed converge to some solution then the  $TV$  must at  
 358 some point plateau so that more oscillations cannot be introduced.

359 This is indeed the findings of the simulations that were run as can be seen by figure 9.  
 360 With the  $TV$  increasing as  $\Delta x$  decreases at the start as the models resolve more and more  
 361 dispersive waves. But as  $\Delta x$  decreases further the  $TV$  plateaus and thus the oscillations are  
 362 not growing without bound. Thus the scheme has not become unstable which supports fur-  
 363 ther that this formulation handles shocks and the resultant dispersive waves well. Also note  
 364 that as expected the higher order the method the higher  $TV$  it has at the start and the faster  
 365 it plateaus and these is very good agreement between the second and third order schemes.  
 366 Although as discussed in (Zoppou and Roberts 1996) second-order schemes will produce  
 367 dispersive errors and thus introduce oscillations, what this demonstrates is that such oscil-  
 368 lations are so small that they are insignificant compared to the resolved oscillations by the  
 369 diffusive errors of the comparable third-order scheme. Thus the move from a second- to  
 370 a third-order method while resolving more of the solution doesn't demonstrate behaviour  
 371 not seen in the second-order solutions.

372 These solutions compare very well to the findings in (El et al. 2006) with both the  
373 second- and third-order schemes resolving the oscillations around the 'contact discontinuity'  
374 (El et al. 2006) between the rarefaction fan and the shock. In (Le Métayer et al. 2010)  
375 it was reported that for their first-order scheme such oscillatory behaviour was not seen  
376 but it can be seen as in Figure 11 with  $\Delta x = 0.00152587890625$ .

## 377 CONCLUSIONS

378 A first-, second- and third-order hybrid finite difference-volume scheme were developed  
379 to solve the Serre equations in conservative form. The schemes were then tested  
380 and validated. Firstly the order of the schemes were all verified, secondly the schemes  
381 shock handling was validated by experimental data. Thirdly the behaviour of the solutions  
382 matched previous findings. Thus it can be concluded that these methods were all  
383 correct and they properly handle shocks. It was also demonstrated that for these equations  
384 second-order although not as accurate as third-order still provides a satisfactory method  
385 for reasonable  $\Delta x$  unlike the first-order method which requires computationally restrictive  
386  $\Delta x$  to produce similar accuracy. This work also validates the findings in (El et al. 2006).[]

## 387 ACKNOWLEDGEMENTS

## 388 REFERENCES

- 389 Carter, J. D. and Cienfuegos, R. (2011). "Solitary and cnoidal wave solutions of the serre  
390 equations and their stability." *European Journal of Mechanics B/Fluids*, 30(3), 259–268.
- 391 El, G., Grimshaw, R. H. J., and Smyth, N. F. (2006). "Unsteady undular bores in fully  
392 nonlinear shallow-water theory." *Physics of Fluids*, 18(027104).
- 393 Godunov, S. K. (1959). "A difference method for numerical calculation of discontinuous  
394 solutions of the equations of hydrodynamics." *Matematicheskii Sbornik*, 89(3), 271–  
395 306.
- 396 Gottlieb, S., Ketcheson, D. I., and Shu, C. W. (2009). "High order strong stability preserving  
397 time discretizations." *Journal of Scientific Computing*, 38(3), 251–289.
- 398 Hammack, J. L. and Segur, H. (1978). "The korteweg-de vries equation and water waves.  
399 part 3. oscillatory waves." *Journal of Fluid Mechanics*, 84(2), 337–358.
- 400 Koren, B. (1993). "A robust upwind discretization method for advection, diffusion and  
401 source terms." *Notes on Numerical Fluid Mechanics*, Vol. 45, Centrum voor Wiskunde  
402 en Informatica, Amsterdam.
- 403 Kurganov, A., Noelle, S., and Petrova, G. (2002). "Semidiscrete central-upwind schemes  
404 for hyperbolic conservation laws and hamilton-jacobi equations." *Journal of Scientific  
405 Computing, Society for Industrial and Applied Mathematics*, 23(3), 707–740.
- 406 Lannes, D. and Bonneton, P. (2009)." *Physics of Fluids*, 21(1), 16601–16610.

- 407 Le Métayer, O., Gavrilyuk, S., and Hank, S. (2010). "A numerical scheme for the green-  
 408      naghdi model." *Journal of Computational Physics*, 229(6), 2034–2045.
- 409 LeVeque, R. (2002). *Finite Volume Methods for Hyperbolic Problems*, Vol. 54 of *Cam-  
 410      bridge Texts in Applied Mathematics*. Cambridge University Press.
- 411 Li, M., Guyenne, P., Li, F., and Xu, L. (2014). "High order well-balanced cdg-fe methods  
 412      for shallow water waves by a green-naghdi model." *Journal of Computational Physics*,  
 413      257, 169–192.
- 414 Su, C. H. and Gardner, C. S. (1969). "Korteweg-de vries equation and generalisations. iii.  
 415      derivation of the korteweg-de vries equation and burgers equation." *Journal of Mathe-  
 416      matical Physics*, 10(3), 536–539.
- 417 Zoppou, C. and Roberts, S. (1996). "Behaviour of finite difference schemes for advection  
 418      diffusion equations." *Technical Report Mathematics Research Report No.MRR 062-96*.

419 **NOTATION**

420      The following symbols are used in this paper:

- $a$  = characteristic order of free surface amplitude;
- $B$  = characteristic order of bottom topography variation;
- $g$  = acceleration due to gravity on earth ( $\text{m}/\text{s}^2$ )
- $h_0$  = characteristic water depth;
- $h$  = water depth (m);
- $L$  = characteristic horizontal scale;
- $p$  = pressure ( $\text{N}/\text{m}^2$ );
- $u$  = fluid particle velocity  $x$ -direction (m/s);
- $w$  = fluid particle velocity  $z$ -direction (m/s);
- $\epsilon$  = nonlinearity parameter  $a/h_0$  ;
- $\xi$  = water depth from free surface (m) ;
- $\sigma$  = shallowness parameter  $h_0^2/L^2$ .

421 **SUBSCRIPTS**

422       $i$  = space discretisation.

423 **SUPERSCRIPTS**

424       $n$  = time discretisation.

425 **ACCENTS**

426       $\bar{q}$  = quantity  $q$  averaged over the depth of water

426       $\bar{\bar{q}}$  = quantity  $q$  averaged over a  $\Delta x$  length interval of space [only make sense given a  $x$  position to cer-

427 **List of Figures**

428 1	The notation used for one-dimensional flow governed by the Serre equation.	16
429 2	Convergence of relative error using L1 norm for analytic soliton solution for both $h$ (○) and $u$ (◇) for first (a), second (b) and third (c) order schemes.	17
430 3	Plotted example soliton simulation for first-order scheme (○) with $dx =$ $1.5625m$ against the analytic solution of (6) (—) with black and blue for $t = 0s$ and $t = 100s$ respectively. . . . .	18
431 4	Plotted example soliton simulation for second-order scheme (○) with $dx =$ $1.5625m$ against the analytic solution of (6) (—) with black and blue for $t = 0s$ and $t = 100s$ respectively. . . . .	19
432 5	Plotted example soliton simulation for third-order scheme (○) with $dx =$ $1.5625m$ against the analytic solution of (6) (—) with black and blue for $t = 0s$ and $t = 100s$ respectively. . . . .	20
433 6	Rectangular wave experiment for first order scheme at $\frac{x}{h_1} : 0$ (a), 50 (b), 100 (c), 150 (d) and 200 (e) . . . . .	21
434 7	Rectangular wave experiment for second order scheme at $\frac{x}{h_1} : 0$ (a), 50 (b), 100 (c), 150 (d) and 200 (e) . . . . .	22
435 8	Rectangular wave experiment for third order scheme at $\frac{x}{h_0} : 0$ (a), 50 (b), 100 (c), 150 (d) and 200 (e) . . . . .	23
436 9	The change in total variation (TV) over $\Delta x$ for first (○), second (□), and third (◇) order schemes. . . . .	24
437 10	Solutions for the dam break problem for first- (a), second- (b) and third- order (c) schemes . . . . .	25
438 11	Solution for the dam break problem for first-order scheme with $\Delta x =$ $0.00152587890625$ . . . . .	26

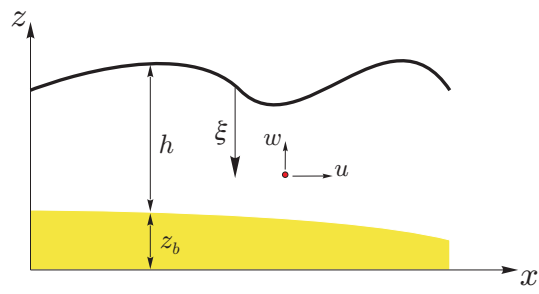


**FIG. 1. The notation used for one-dimensional flow governed by the Serre equation.**

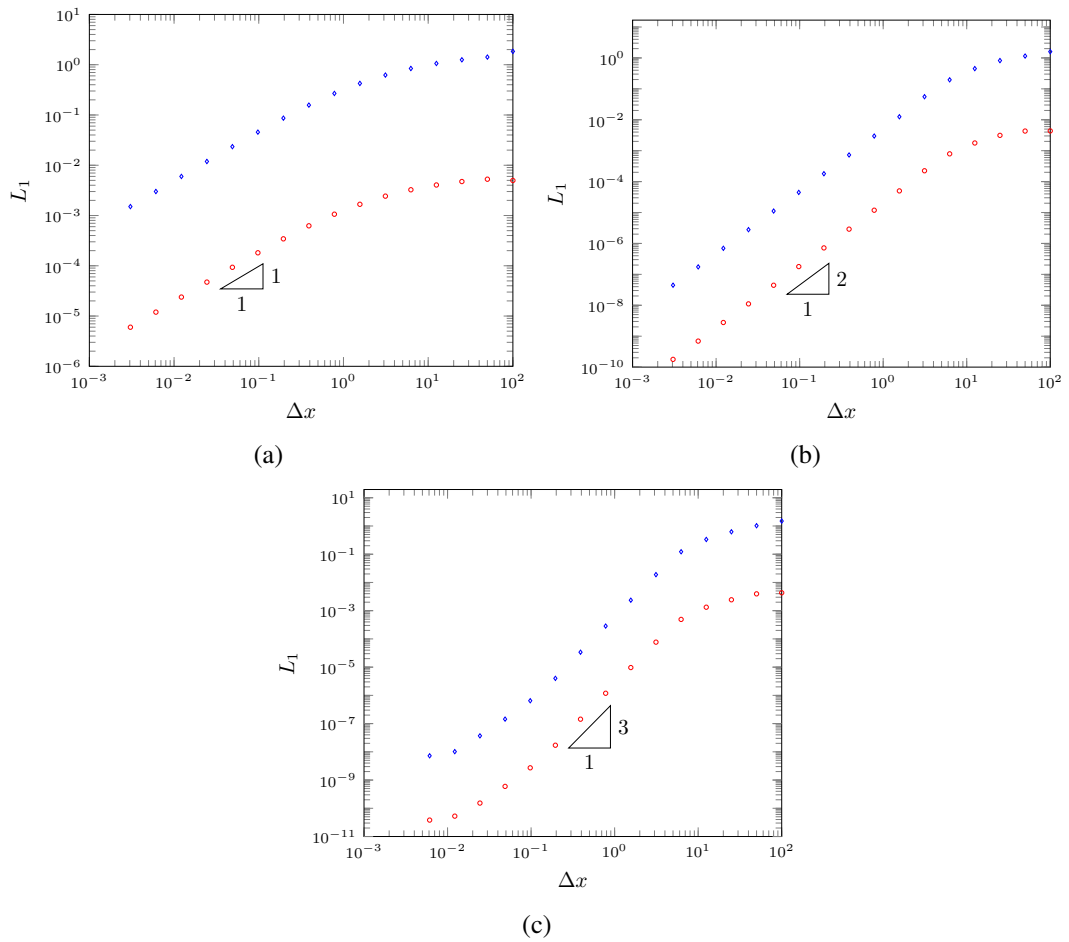


**FIG. 2. Convergence of relative error using L1 norm for analytic soliton solution for both  $h$  ( $\circ$ ) and  $u$  ( $\diamond$ ) for first (a), second (b) and third (c) order schemes.**

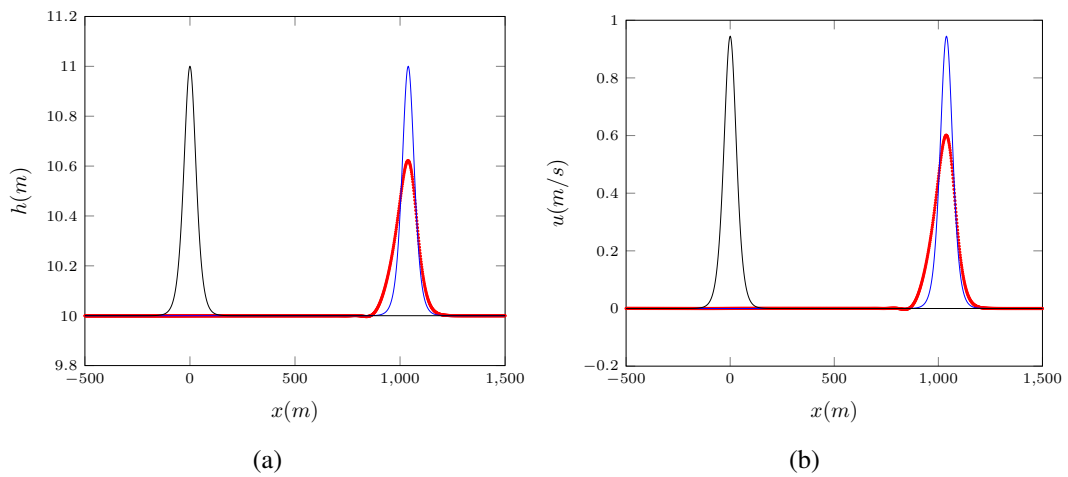


**FIG. 3. Plotted example soliton simulation for first-order scheme ( $\circ$ ) with  $dx = 1.5625m$  against the analytic solution of (6) (—) with black and blue for  $t = 0s$  and  $t = 100s$  respectively.**

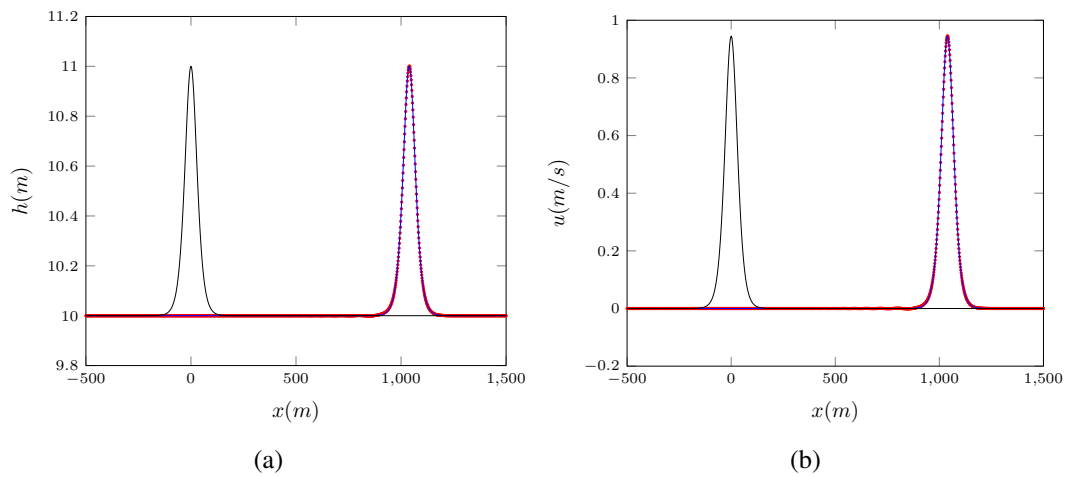


**FIG. 4. Plotted example soliton simulation for second-order scheme ( $\circ$ ) with  $dx = 1.5625m$  against the analytic solution of (6) ( $-$ ) with black and blue for  $t = 0s$  and  $t = 100s$  respectively.**

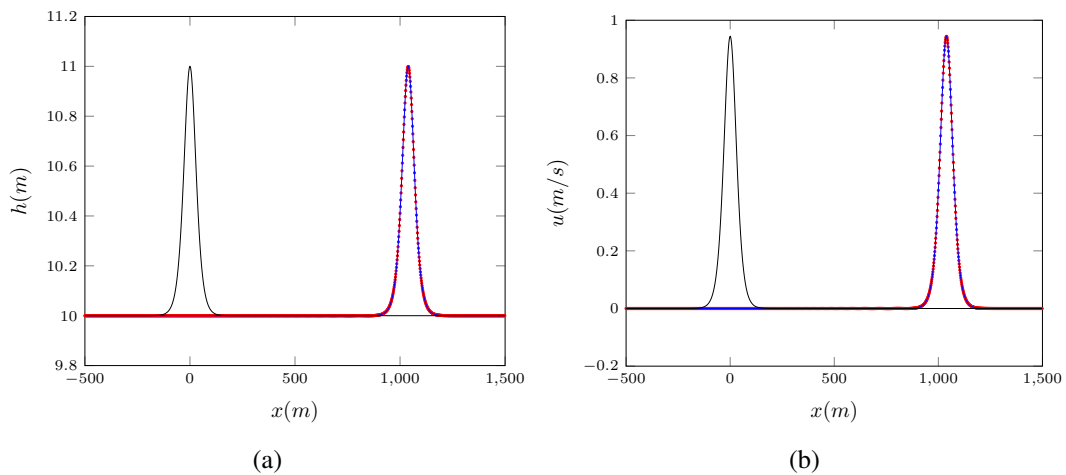


**FIG. 5.** Plotted example soliton simulation for third-order scheme ( $\circ$ ) with  $dx = 1.5625m$  against the analytic solution of (6) ( $-$ ) with black and blue for  $t = 0s$  and  $t = 100s$  respectively.

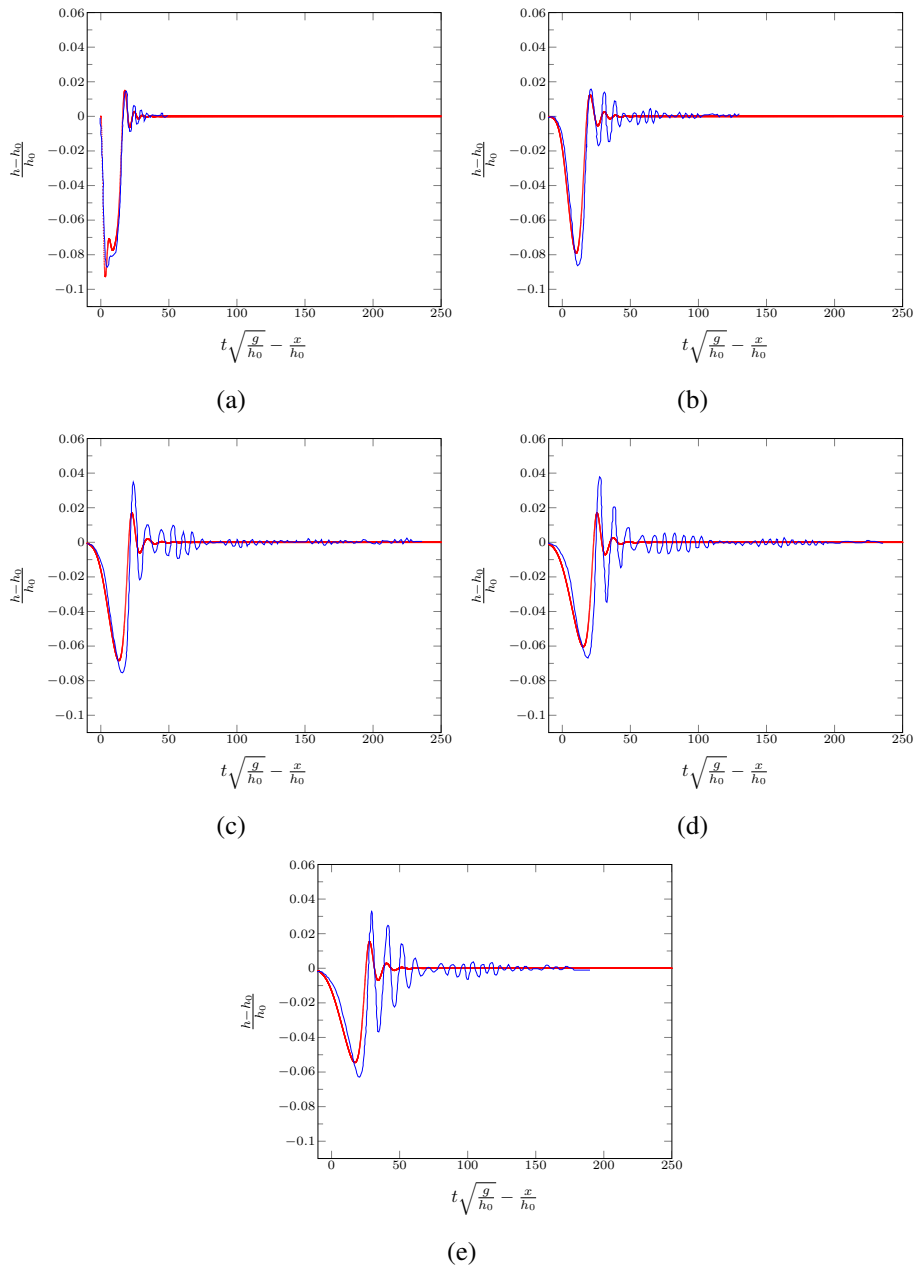


**FIG. 6. Rectangular wave experiment for first order scheme at  $\frac{x}{h_1} : 0$  (a), 50 (b), 100 (c), 150 (d) and 200 (e)**

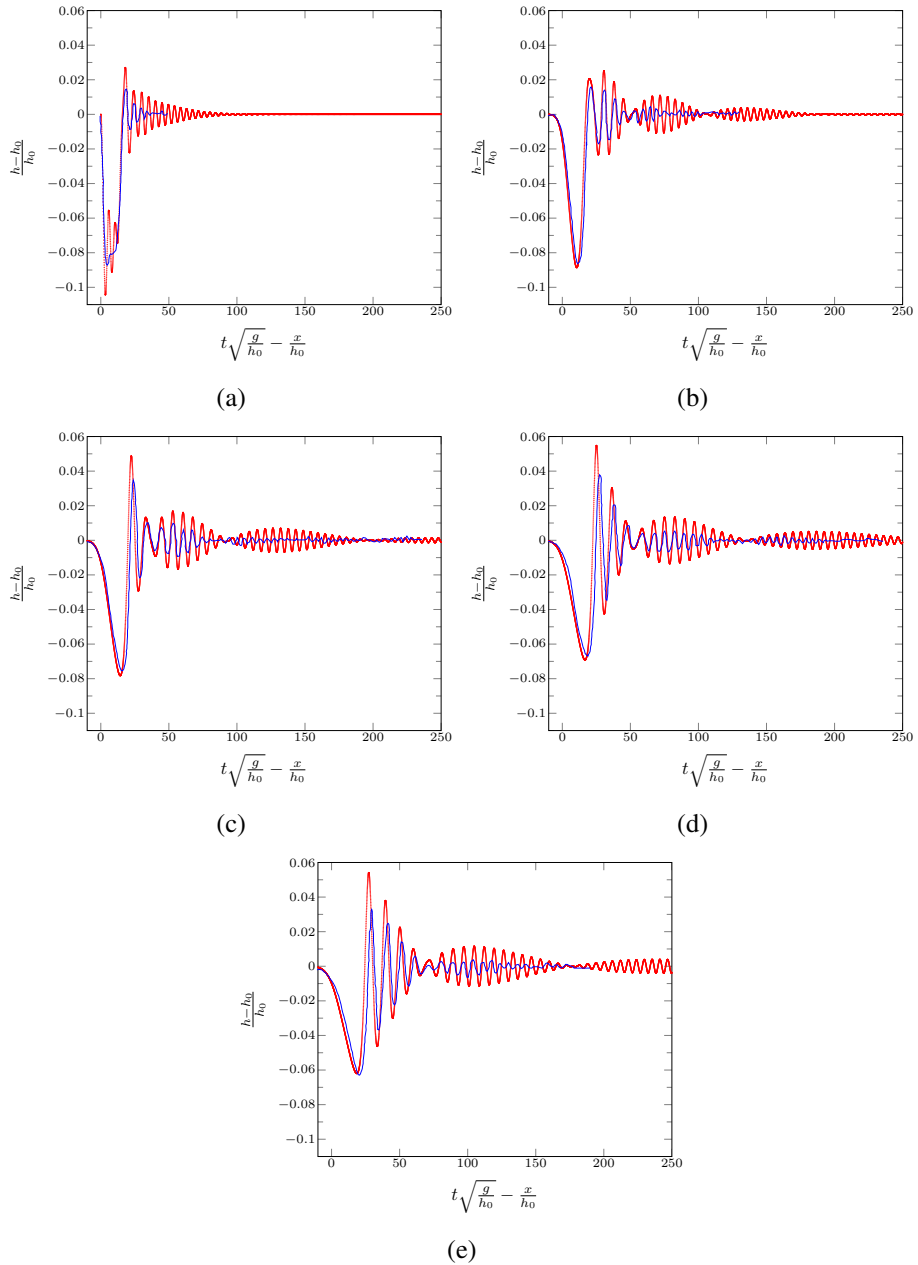


**FIG. 7. Rectangular wave experiment for second order scheme at  $\frac{x}{h_1} : 0$  (a), 50 (b), 100 (c), 150 (d) and 200 (e)**

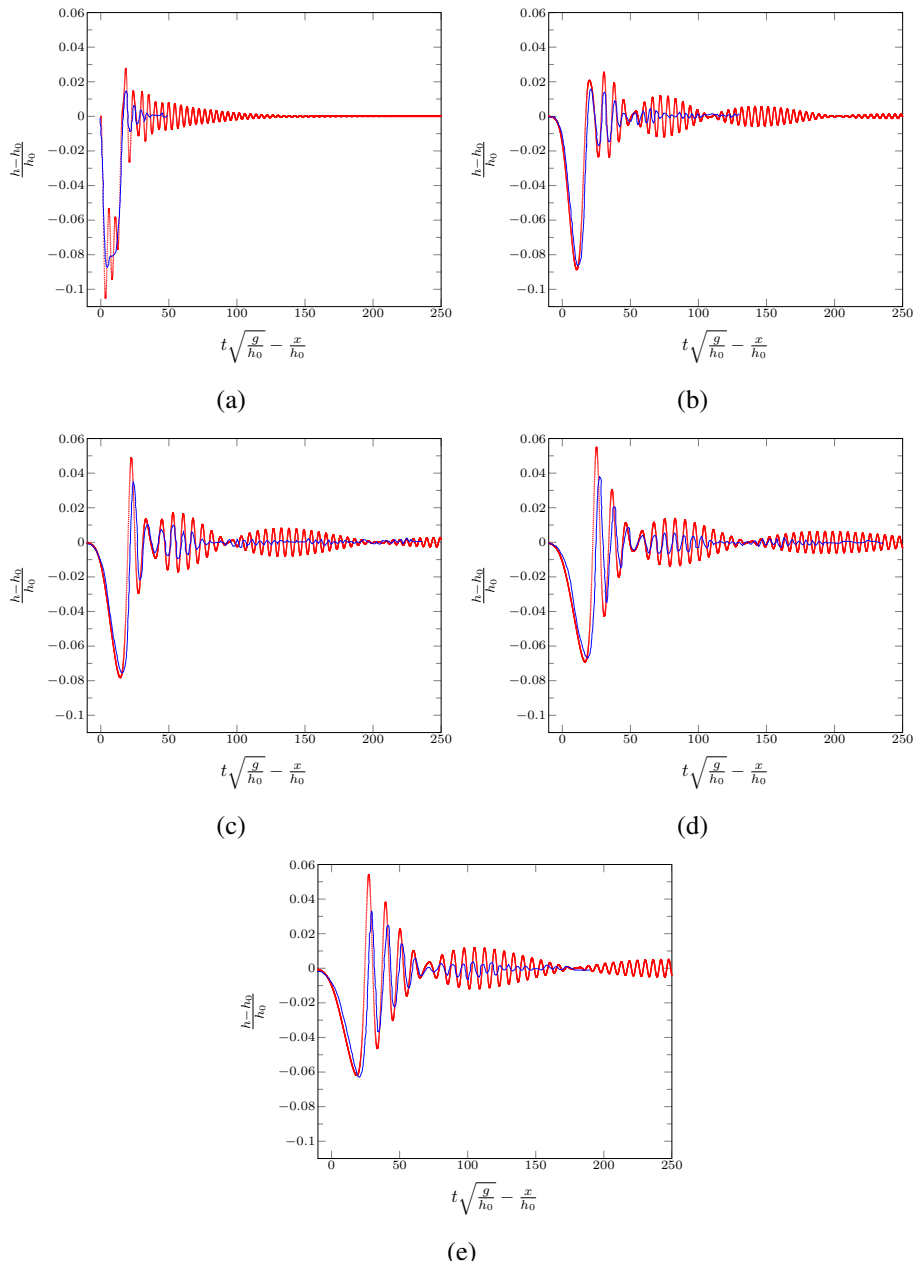


**FIG. 8. Rectangular wave experiment for third order scheme at  $\frac{x}{h_0} : 0$  (a), 50 (b), 100 (c), 150 (d) and 200 (e)**

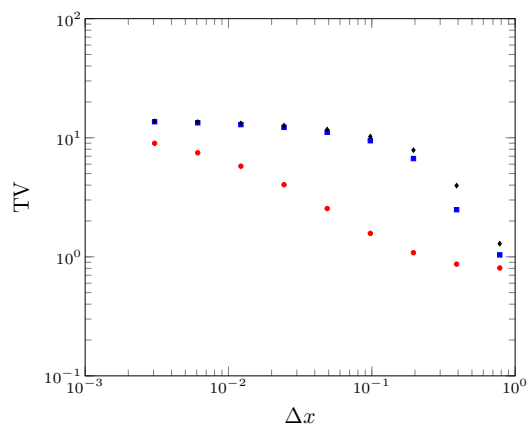


**FIG. 9. The change in total variation (TV) over  $\Delta x$  for first ( $\circ$ ) , second ( $\square$ ), and third ( $\diamond$ ) order schemes.**

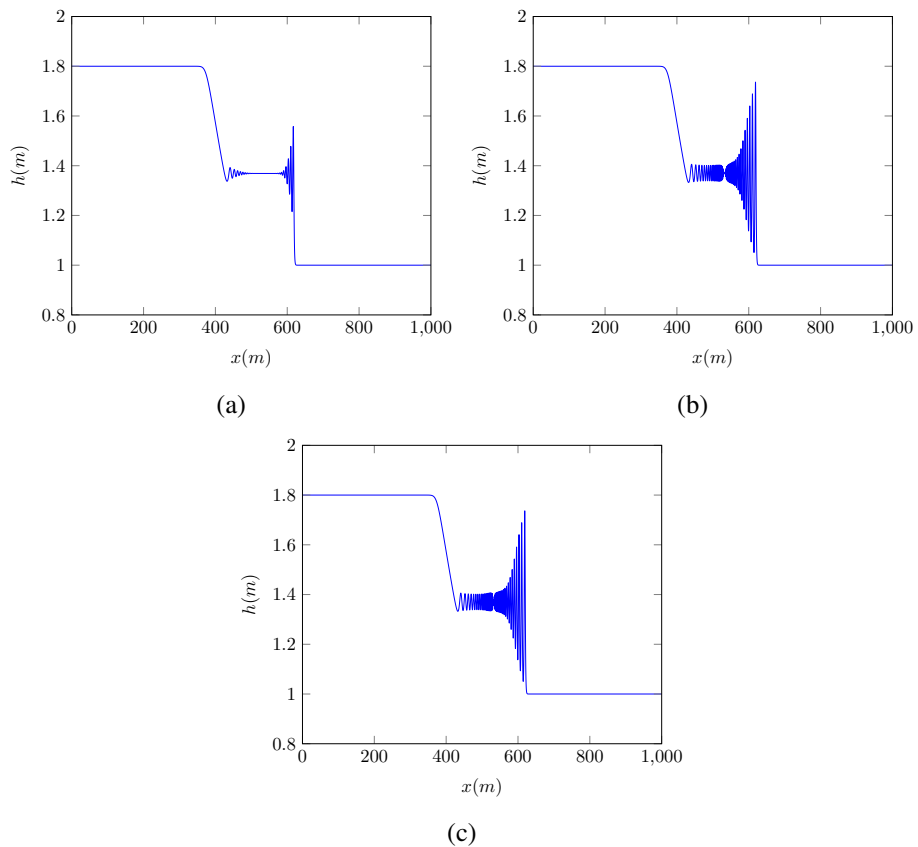


**FIG. 10. Solutions for the dam break problem for first- (a), second- (b) and third-order (c) schemes**

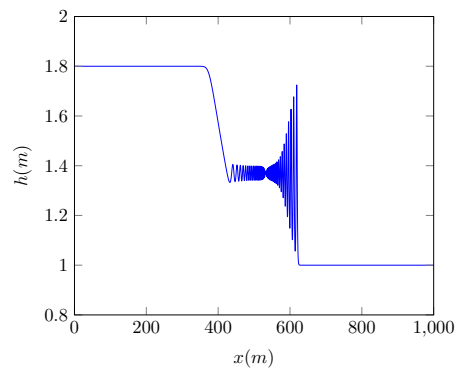


**FIG. 11. Solution for the dam break problem for first-order scheme with  $\Delta x = 0.00152587890625$**